Computational Materials Science 112 (2016) 342–346

Contents lists available at ScienceDirect

Computational Materials Science

journal homepage: www.elsevier.com/locate/commatsci

A first-principles study of the mechanical properties of AlN with Raman verification

Yiquan Dai [a], Weihui Wang [a], Chengqun Gui [b], Xiaodong Wen [c,d], Qing Peng [b,e], Sheng Liu [b,*]

[a] Mechanical Sci. & Eng., Huazhong University of Science & Technology, Wuhan 430074, China
[b] Cross-disciplinary Institute of Engineering Sciences, School of Power and Mechanical Engineering, Wuhan University, Wuhan, Hubei 430072, China
[c] State Key Laboratory of Coal Conversion, Institute of Coal Chemistry, Chinese Academy of Sciences, Taiyuan 030001, China
[d] Synfuels China Co. Ltd Huairou, Beijing 101407, China
[e] Department of Mechanical, Aerospace and Nuclear Engineering, Rensselaer Polytechnic Institute, Troy, NY 12180, USA

ARTICLE INFO

Article history:
Received 19 May 2015
Received in revised form 25 August 2015
Accepted 12 September 2015
Available online 21 November 2015

Keywords:
Mechanical constants
First principle calculation
Raman scattering

ABSTRACT

We report calculation to rebuild Raman frequencies detected in Raman scattering of high quality wurtzite-type AlN bulk single crystal. Then, we use this Raman verified mode and parameters to calculate mechanical constants and phonon pressure coefficients, which are all important parameters in Raman based stress detection. The relationship between the modes used in Raman rebuilding and constants calculation are discussed in detail. We have predicted for the first time $2\tilde{a}+\tilde{b}$ under different pressures. We have oberserved a new trend that $2\tilde{a}+\tilde{b}$ is decreasing slightly according to the pressure, oppose to a constant as assumed. This work is a good foundation for stress/strain analysis used in film and device reliability testing.

1. Introduction

Aluminum nitride (AlN) is a wide band gap (6.01–6.05 eV at room temperature) semiconductor material, with potential applications as the core of various key technologies including MIS (metal–insulator–semiconductor) devices [1]. AlN is widely used in mobile phone Radio Frequency filters [2] and Ultra–Violet solid state light sources [3]. In spite of remarkable progress in the growth of III-nitride films and device fabrication technologies, some basic properties of AlN remain poorly studied, especially those related to monitoring techniques for mass production and reliability testing techniques for micro scale devices. In focus of these problems, lattice mismatch and thermal mismatch between film and substrate [4,5] cause large strain, which leads to high dislocation density or even cracking [6]. Directly measuring engineering strain states of these micro scale semiconductors is one of the key techniques required nowadays.

Experimentally, Raman scattering is widely used as a convenient and nondestructive strain detection method. Raman active phonons are straightforward signatures of bonds to sample strain fields, phase mixing, and interface morphologies. The quality of film crystallization and its in-situ evolution can also be characterized by Raman scattering [7]. Theoretically, Raman frequencies are in general calculated by density functional perturbation theory (DFPT) (also termed as Linear Response method) [8].

There are extensive studies of mechanical constants [9–12] and phonon deformation potentials [13–17] by first-principles calculations. Most results do not agree with experimentally detected Raman frequencies. Moreover, most of the investigators neglect to report whether or not their results are consistent with Raman frequencies. In fact, the phonon spectrum from Raman scattering is one of the fundamental indicators for crystal dynamics [18], which in turn works as a bridge between mechanical constants and Raman frequencies. Specially, recent publications of Łepkowski [11] and Callsen et al. [14] reveal that some elastic stiffness constants are sensitive to Raman frequency shifts and calculation methods. The main difficulties might be the high accuracy of elastic constants calculations. While the main idea of elastic constants determination [9,10] is by setting a finite value as stress/strain and then calculating corresponding strain/stress after re-minimizing the total energy, the two calculations have some intrinsic relationship all based on total energy which is mainly comprised of potential energy and kinetic energy. Considering the Born–Oppenheimer approximation (Temperature → 0 K), the kinetic energy should be zero. This implies that the kinetic energy error is a strong function of E_{cut} (scaling as E_{cut}^{-4}) [19]. Moreover, this small error in the value of E_{cut} will further lead to greater errors in the elastic constants and Raman spectra calculations due to the derivative operation of total energy. As a result, a quantitative

* Corresponding author.
E-mail address: victor_liu63@126.com (S. Liu).

http://dx.doi.org/10.1016/j.commatsci.2015.09.027
0927-0256/

prediction of Raman frequencies from first-principles calculations agreeing well with experiments is still lacking but desirable for further implication of Raman based measurement, such as, film growth monitoring and stress detection.

This study aims to rebuild Raman frequencies and predict the mechanical properties from first-principles calculations. The computational method is detailed in Section 2. The results are in Section 3, followed by conclusion in Section 4.

2. Methodology

The first-principles calculations have been done using CASTEP (Cambridge Sequential Total Energy Package [20]), by which the DFT scheme within the GGA approximation is carried out. The well established Perdew–Wang (PW91) version of the GGA approximation is adopted and norm-conserving pseudopotentials are used to describe electron-ion interactions.

The plane-wave energy cut-off, E_{cut}, is 120 Ry (1632 eV) and Monkhorst–Pack grids of $11 \times 11 \times 11$ are used for Brillouin Zone (BZ) sampling (FFT grid density is $45 \times 45 \times 72$). The geometry optimizations are achieved while the maximum force on every atom is smaller than 3.0×10^{-7} eV/Å; Additionally, norm-conserving pseudopotentials are adopted for considering the weak crystal symmetry and inhomogeneous electron gas distribution of AlN. Raman frequencies are calculated by a hybrid finite displacement/density functional perturbation theory (DFPT) [8, 21].

In addition to the GGA-PW91 calculations above, calculations based on the local density approximation (LDA) are also performed. The convergence thresholds used in the geometry optimizations and all other settings are kept as above.

There are mainly three variables related to stress/strain and polarization analyses, the biaxial modulus $\overline{C}$, bulk modulus B and Poisson ratio γ_{zx}, which are calculated by [9,13]

$$\begin{cases} \overline{C} = C_{11} + C_{12} - 2\frac{C_{13}^2}{C_{33}} \\ \sigma_{xx} = \overline{C}\varepsilon_{xx} \\ B = \dfrac{(C_{11}+C_{12})C_{33} - 2C_{13}^2}{C_{11}+C_{12}+2C_{33}-4C_{13}} \\ \gamma_{zx} = \dfrac{C_{13}}{C_{11}+C_{12}} \end{cases} \quad (1)$$

where C stands for elastic constant, B stands for bulk modulus, γ_{zx} stands for Poisson ratio, σ and ε stand for stress and strain tensors.

2.1. Convergence tests

E_{cut} is not usually known in advance for given calculation. Therefore, trying increased values of E_{cut} and inspecting the change of total energy to be small enough is one of the two important convergence tests, see Fig. 1.

BZ sampling is realized by the Monkhorst–Pack method [22], which is an important bridge to treat the electronic structure for periodic systems in that it is able to take advantage of translational symmetry through Bloch's theorem with a finite number of k-points rather than full integration over the BZ [19]. Therefore, the approximation with a finite number of k-points should also be verified by convergence tests (see Fig. 2).

It is worth mentioning that there is a balanced input for total energy minimization. As shown in Figs. 1 and 2, we attempt to explore balanced E_{cut} and k-points for total energy minimization. The slopes of the total energy changing in Fig. 1 (4.738×10^{-6}) and Fig. 2 ($\times 10^{-6}$) are more or less in the same order of magnitude. At the same time, curvilinear trends in figures show an obvious difference. Therefore, well designed fitting functions are also shown in both figures to extrapolate the slope between total energy and

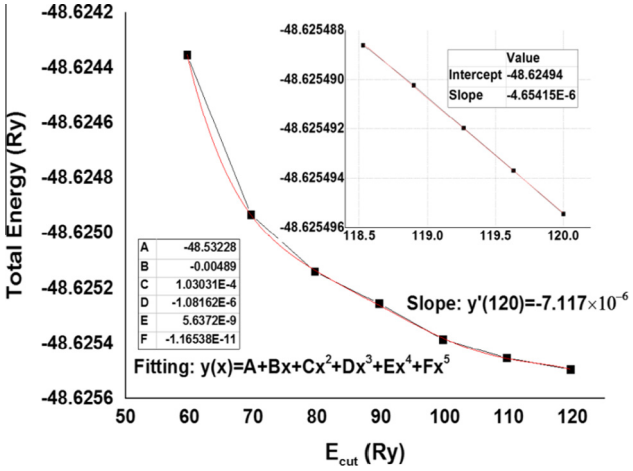

Fig. 1. Convergence test of E_{cut}.

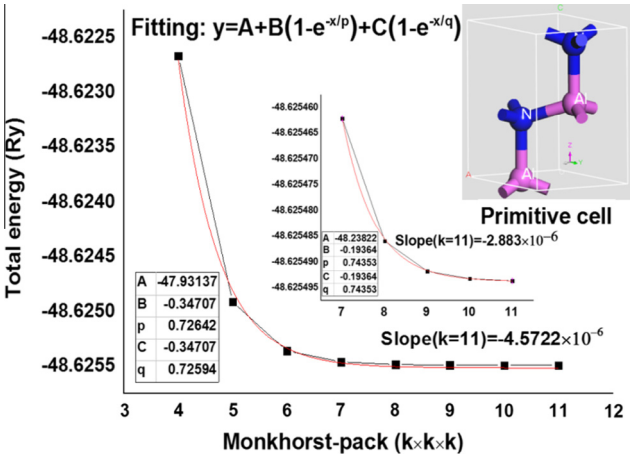

Fig. 2. Convergence test of k-point grid.

E_{cut} or k-points. In fact, the four total energy related items, E_{cut}, k-points, SCF tolerance, and convergence thresholds in energy minimization, should be selected carefully with balanced control for a good final precision but with less computational cost.

3. Results and analysis

Wurtzite-type AlN belongs to the C_{6v}^4 ($P6_3mc$) space group [23], with two formula units and four atoms per primitive cell. The primitive cell information used as original input is from ICSD#41482 [24]. After geometry optimizations, the lattice parameters are $a = 3.073$ Å, $c = 4.948$ Å, and $u = 0.381$, and $a = 3.064$ Å, $c = 4.925$ Å, and $u = 0.381$ for GGA and LDA calculations, respectively.

There are six optical modes: $\Gamma = A_1 + E_1 + 2E_2 + 2B_1$ [25]. A_1 and E_1 are both infrared and Raman active (polarized along z (c-lattice) optical axis and in the basal (x,y) plane respectively). At the same time, both of them will split into LO and TO frequencies. Short-range atomic forces and long-range Coulomb fields are responsible for $A_1 - E_1$ and LO–TO splitting respectively [26]. This provides an insight for the calculation methods selection (e.g., LDA or GGA). Additionally, E_2 (E_2^{low} and E_2^{high}, none polarized) modes are Raman active and $2B_1$ are silent modes without meaning in practical stress detection.

Table 1
Comparison with Raman experiments (unit: cm^{-1}).

Refs.	E_2^{low}	$A_1(TO)$	E_2^{high}	$E_1(TO)$	More info.
[27]		611	657	671	Bulk crystal, FWHM(E_2^{high}) < 3.8 cm^{-1}
[28]		609.6	656	669.3	Bulk crystal, FWHM(E_2^{high}) ≈ 6.6 cm^{-1}
[13]	247.5	608.5	655.5	669.3	Bulk crystal (whisker)
[13]	241	618	667	677	Calculated, LDA, E_{cut} = 75 Ry
[29]	237	594	636	649	Calculated, GGA–PBE, E_{cut} = 60 Ry
[25]	252	615	667	673	Calculated, E_{cut} unknown
[25]	248.4	613.8	660	673.4	T = 6 K, film on α-Al_2O_3
[25]	248.6	611.0	657.4	670.8	T = 300 K, film on α-Al_2O_3
LDA	243.6	629.2	672.3	684.2	Calculated, LDA, E_{cut} = 120 Ry
GGA	247.3	615.6	656.5	670.5	Calculated, GGA–PW91, E_{cut} = 120 Ry

According to [25], frequencies change little between 6 K (∼0 K, ground state) and 300 K.

We summarize our results of Raman frequencies and compared to experiments in Table 1:

FWHM (Full Width at Half Maximum) line-width in Raman spectra is widely recognized as an inversely proportional indicator of phonon lifetime [25], which in turn denotes higher crystal quality with longer phonon lifetime. According to this, bulk crystal from [27] is the best one among these carefully selected references (according to their bulk crystal quality). Thus, it is reasonable to take its frequencies as a benchmark for comparison here. As can be seen in Table 1, our calculated results show excellent agreement with frequencies from high quality bulk crystal [27]. The only flaw appeared in A_1(TO) with a difference of $615.6 - 611 = 4.6\ cm^{-1}$ between the calculated and benchmark frequencies. In order to give a detailed discussion on this and later Raman implications on stress detection, some space group information of AlN is necessary here.

In practical implication, strong narrow peak in E_2^{high} has the best prospect in strain/stress detection for nitride compounds due to its lack of polarization that resists geometry alignment errors in testing [27]. (The intensity of another non-polarized phonon, E_2^{low} is much lower). Other polarized phonons are easy to influence in detection, especially by the angle/rotation of incident light [30]. Therefore, A_1(TO) (polarized) may be influenced (reflected) by substrates or other crystal faces due to deviation from the ideal geometry arrangement during Raman detection [31]. Another unverified trend we found is the phonon frequencies with lower quality show a lower shift compared with higher quality bulk crystal, see Raman frequencies from [27] and [28] in Table 1 for example. This could explain the small deviation of A_1(TO) of bulk crystal in our calculations.

After verification with Raman experimentation, the elastic constants are also calculated with the same mode and energy minimization parameters, as summarized in Table 2.

The elastic constants predicted in Refs. [11,12] (see Table 2) both based on LDA show a good agreement with each other, but not experiment. On the contrary, although the Raman frequencies from our LDA calculations (in Table 1) have considerable difference with experimental data – especially the reliable experimental phonon E_2^{high} – the elastic constants agree well with experiments (Table 2), even better than GGA from which the structure is able to rebuild Raman frequencies very well in Table 1. It is widely recognized that lattice parameters will increase if GGA is adopted as the exchange–correlation functional in geometry optimizations. However, the lattice constants decrease in our calculation compared with experimental lattice constants. At the same time, Raman frequencies calculated with the same exchange–correlation functional and optimized structure compare well with experiment. This makes it worthy to explore mechanisms for additional compounds in terms of pseudopotential design and geometry optimization algorithm improvements.

It is worth noting that though Raman frequencies calculated by LDA are not as acceptable as GGA-PW91 using norm-conserving pseudo potentials, the difference in calculated elastic constants is not so obvious compared with experiment ones as shown in Table 2, considering difficulty in evaluation of experiment error. Theoretically, Raman frequency and elastic constant calculations are based on second and first order derivative operations of the total energy respectively. In this viewpoint, elastic constants calculated by GGA-PW91 are more reasonable.

Here the phonon pressure coefficients are considered, which are also necessary in Raman stress/strain detection. Under the framework of Hooke's law, phonon pressure coefficients are defined [14] as the proportion between Raman frequency shift $\Delta\omega_\lambda$ and strain/stress (λ is indicator of the selected phonon. As mentioned above, E_2^{high} is the first choice in practical application.):

$$\Delta\omega_\lambda = 2a\varepsilon_{xx} + b\varepsilon_{zz} = 2\tilde{a}\sigma_{xx} + \tilde{b}\sigma_{zz} \tag{2}$$

where ε and σ are the strain and stress tensors respectively. The constants a, b, $\tilde{a}$, and $\tilde{b}$ are the coefficients. There is a reasonable assumption for common AlN thin films on different substrates: $\varepsilon_{xx} = \varepsilon_{yy}$ and $\sigma_{xx} = \sigma_{yy}$.

The idea for determining these coefficients is to impose a known stress/strain condition to the studied system, followed with total energy minimization, and then calculate the corresponding

Table 2
Calculated elastic constants (unit: GPa).

Refs.	C_{11}	C_{12}	C_{13}	C_{33}	C_{44}	$\overline{C}$	B	γ_{zx}
LDA [11]	397	144	115	372	115	469.9	211.9	0.2126
LDA [12]	401	143	112	369	118	476.0	210.6	0.2059
GGA [14]	361	130	93	339	107	440.0	187.1	0.1894
Expt. [32]	411	149	99	389	125	509.6	210.4	0.1768
Expt. [33]	390 ± 15	145 ± 20	106 ± 20	398 ± 20	105 ± 10	478.5	210.0	0.1981
Expt. [34]	410.5	148.4	98.9	384.3	124.0	508.0	209.5	0.1770
LDA	411.5	136.9	101.8	402.5	123.0	496.9	211.4	0.1856
GGA	408.4	124.0	90.7	401.2	125.4	491.4	202.8	0.1704

Table 3
Hydrostatic-pressure and calculated $2\tilde{a}+\tilde{b}$ (unit: cm^{-1}/GPa).

Pressure	E_2^{low}	A_1(TO)	E_2^{high}	E_1(TO)	Peak-$E_2^{high}(cm^{-1})$
−5.0	0.0651	5.0441	6.1916	5.6571	625.5646
−1.5	0.0427	5.0133	6.1130	5.5973	647.3532
−0.5	0.0364	5.0005	6.0913	5.5817	653.4770
0.5	0.0307	4.9966	6.0720	5.5673	659.5587
1.5	0.0257	4.9910	6.0536	5.5525	665.6031
5.0	0.0081	4.9632	5.9902	5.5050	686.4735
Average	**0.0348**	**5.0015**	**6.0853**	**5.5768**	
[13]	0.12 ± 0.05	4.4 ± 0.1	4.99 ± 0.3	4.55 ± 0.03	Expt. $2\tilde{a}+\tilde{b}$
[14]	0.75 ± 0.04	1.46 ± 0.02	1.66 ± 0.02	1.20 ± 0.02	Expt. $\tilde{b}$
[29]	0.07 ± 0.02	4.35 ± 0.03	5.40 ± 0.04	5.33 ± 0.04	Expt. $2\tilde{a}+\tilde{b}$

(1) Pressure > 0 means being compressed; (2) Considering that other phonons are easy to be influenced in detection, we should pay more attention on E_2^{high}; (3) We have evaluated AlN films with different substrates appeared in recent years (including sapphire, SiC, Si (0 0 1) and ourselves experiment on Si (1 1 1)), stress in film on Si (1 1 1) substrate is the largest, more or less 2.0 GPa, thus, we did not calculate more higher pressure status.

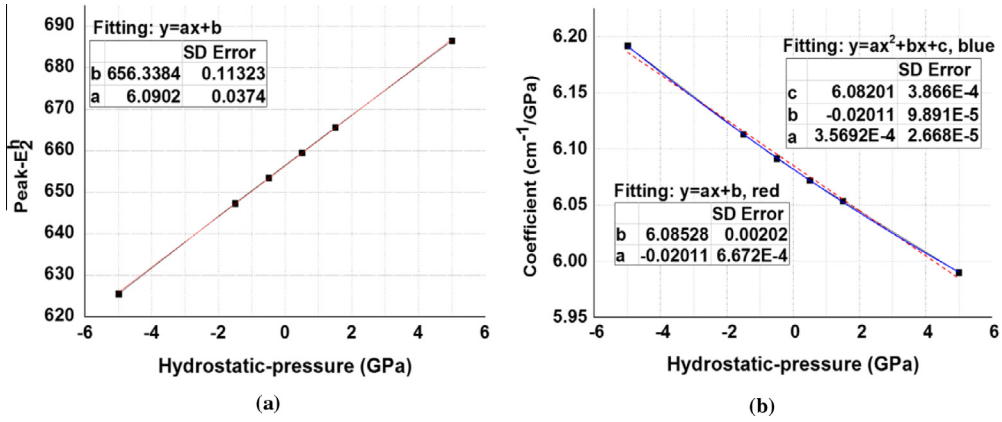

Fig. 3. Curves of Hydrostatic-pressure between Peak of E_2^{high} and $2\tilde{a}+\tilde{b}$.

frequency shift $\Delta\omega$ to determine the constants by formula (1) [9,14]. For example [14]:

$$\begin{cases} \sigma_{xx}=\sigma_{yy}=0, \sigma_{zz}\neq 0 \Rightarrow \Delta\omega \sim \tilde{b} \ \textit{uniaxial pressure} \\ \sigma_{xx}=\sigma_{yy}=\sigma_{zz}\neq 0 \Rightarrow \Delta\omega \sim 2\tilde{a}+\tilde{b} \ \textit{hydrostatic pressure} \end{cases} \quad (3)$$

A similar process for a and b can be found in [9]. However, what we want to emphasize is that, if the uniaxial-pressure condition is imposed on the model, the cell will not retain its symmetry or else it would be unstable, which means a computational cost greater than the high symmetry crystal calculation but yielding lower precision (The hydrostatic-pressure condition could be imposed without destroying crystal symmetry). Results from experiment under uniaxial-pressure conditions maybe more dependable and could be used to ascertain $\tilde{b}$. Thus, we just calculate the value of $2\tilde{a}+\tilde{b}$ as shown in Table 3.

For the first time in the literature, we calculated $2\tilde{a}+\tilde{b}$ under different pressures (similar studies in the literature only give one coefficient as constant). Correspondingly, we find a new trend never reported before: $2\tilde{a}+\tilde{b}$ is decreasing slightly according to the pressure, as shown in Fig. 3. Commonly, this coefficient is considered a constant with pressure. Therefore, we also list peaks of E_2^{high} in the right highlighted column for further correction. For example, if a detected peak of E_2^{high} is 662 cm^{-1}, a suitable coefficient can be found between 6.0720 and 6.0536 by interpolation.

4. Conclusions

In conclusion, we successfully explored modes and parameters to rebuild Raman frequencies detected from a perfect single crystal, and then, use this Raman verified mode to investigate properties of AlN, specifically aimed at future stress/strain and polarization analyses of AlN films or micro semiconductor devices by Raman detection. We have predicted for the first time $2\tilde{a}+\tilde{b}$ under different pressures. We have oberserved a new trend that $2\tilde{a}+\tilde{b}$ is decreasing slightly according to the pressure, oppose to a constant as assumed. Our study is useful in stress-strain analysis in film and device reliability testing.

Acknowledgement

This work is supported by National Hightech Program (863) with contract number of SS2015AA041802.

References

[1] T. Adam, J. Kolodzey, C.P. Swann, et al., Appl. Surf. Sci. 175 (2001) 428–435.
[2] H.P. Loebl, C. Metzmacher, R.F. Milsom, et al., J. Electroceram. 12 (1–2) (2004) 109–118.
[3] Y. Taniyasu, M. Kasu, T. Makimoto, Nature 441 (7091) (2006) 325–328.
[4] P. Liu, A. De Sarkar, R. Ahuja, Comput. Mater. Sci. 86 (2014) 206–210.
[5] I. Bryan, A. Rice, L. Hussey, Z. Bryan, et al., Appl. Phys. Lett. 102 (6) (2013) 061602.
[6] S. Raghavan, J.M. Redwing, Group III-A Nitrides on Si: Stress and Microstructural Evolution, CRC Press, Boca Raton, 2011.
[7] M. Kuball, Surf. Interface Anal. 31 (10) (2011) 987–999.
[8] S. Baroni, S. De Gironcoli, A. Dal Corso, et al., Rev. Mod. Phys. 73 (2) (2001) 515.
[9] J.-M. Wagner, F. Bechstedt, Phys. Rev. B 66 (11) (2002) 115202.
[10] A.F. Wright, J. Appl. Phys. 82 (6) (1997) 2833–2839.
[11] S.P. Łepkowski, J. Appl. Phys. 117 (10) (2015) 105703.
[12] B.P. Pandey, V. Kumar, E.M. Proupin, Pramana 83 (3) (2014) 413–425.
[13] A.R. Goni, H. Siegle, K. Syassen, et al., Phys. Rev. B 64 (3) (2001) 035205.
[14] G. Callsen, M.R. Wagner, J.S. Reparaz, et al., Phys. Rev. B 90 (20) (2014) 205206.
[15] A. Sarua, M. Kuball, J.E. Van Nostrand, Appl. Phys. Lett. 81 (8) (2002) 1426–1428.

[16] J. Gleize, M.A. Renucci, J. Frandon, E. Bellet-Amalric, et al., J. Appl. Phys. 93 (4) (2003) 2065–2068.
[17] T. Kallel, M. Dammak, J. Wang, et al., Mater. Sci. Eng., B 187 (2014) 46–52.
[18] M. Born, K. Huang, Dynamical theory of crystal lattices, 1954.
[19] A.E. Mattsson, P.A. Schultz, M.P. Desjarlais, et al., Modell. Simul. Mater. Sci. Eng. 13 (1) (2005) R1.
[20] M.D. Segall, P.J.D. Lindan, M.J. Probert, et al., J. Phys. Condens Matter 14 (2002) 2717–2744.
[21] X. Gonze, Phys. Rev. B 55 (16) (1997) 10337.
[22] H.J. Monkhorst, J.D. Pack, Phys. Rev. B 13 (12) (1976) 5188.
[23] C.A. Arguello, D.L. Rousseau, S.P.D.S. Porto, Phys. Rev. 181 (3) (1969) 1351.
[24] Y.N. Xu, W.Y. Ching, Phys. Rev. B 48 (7) (1993) 4335.
[25] V.Y. Davydov, Y.E. Kitaev, I.N. Goncharuk, et al., Phys. Rev. B 58 (19) (1998) 12899.
[26] F. Demangeot, J. Frandon, M.A. Renucci, et al., MRS Internet J. Nitride Semicond. Res. 1 (1996) e23.
[27] W. Zheng, R. Zheng, F. Huang, et al., Photon. Res. 3 (2) (2015) 38–43.
[28] D. Zhuang, J.H. Edgar, B. Liu, H.E. Huey, et al., J. Crst. Growth 262 (1) (2004) 168–174.
[29] F.J. Manjón, D. Errandonea, A.H. Romero, et al., Phys. Rev. B 77 (20) (2008) 205204.
[30] L. Bergman, M. Dutta, C. Balkas, et al., J. Appl. Phys. 85 (7) (1999) 3535–3539.
[31] H. Harima, J. Phys.: Condens. Matter 14 (38) (2002) R967.
[32] L.E. McNeil, M. Grimsditch, R.H. French, Am. Ceram. Soc. 76 (1993) 1132.
[33] A. Polian, M. Grimsditch, I. Grzegory, J. Appl. Phys. 79 (6) (1996) 3343–3344.
[34] R.R. Reeber, K. Wang, MRS Internet J. Nitride Semicond. Res. 6 (2001) e3.